Chapter 6

Discussions

Seismic inversion methods are used for analyzing seismic and well log data to identify hydrocarbon-bearing resources. The aim of the inversion is to locate the anomalous zone from seismic data. This anomalous zone contains hydrocarbon sand with a low impendence value as compared to the neighboring shale. As the sand reservoir is thin, it is difficult to identify the respective reservoir limit in the data. Though the location, thickness, elastic parameter, porosity, density, P-wave and gamma ray of the anomalous zone can be established from the correlation between the seismic and well log data. In the present study, internal and external attributes have been added to the data set for an in-depth understanding of reservoir detection by a number of inversion methods.

6.1 Post-stack inversion

The post-stack inversion has been done on the F3 block, the Netherlands. All four inversion methods (MBI, CI, MLSSI and BLI) have been found to provide similar trends but at different confidence levels, based on the degree of correlation and residual average error values. These methods have been closely scrutinized at the well locations to compare the inverted results of the P- impedance with the log impedance. From the scrutiny of results, it is discernible that MBI has yielded the best correlation results

while CI yielded the least correlation among the four inversion methods. This reveals that MBI provides better amplitude correlation, lower average impedance values, the best vertical resolution and clearly detects the geological inconsistencies in the horizontal layers than the other three inversion methods. The reason behind the accuracy of MBI performance may be attributed to the fact that the acoustic impedance model is altered iteratively until the difference between the inverted trace and the seismic trace is reduced to a threshold value.

Figure 6.1 provides visual overview of all post-stack inversion methods (Crossline 600-900, Inline 244). For convenience, inverted impedance cross sections have been represented between 1500ms to 1850ms time intervals which contains the anomalous zone.The low impedance zone has been highlighted by the arrows in the figures for each inversion method between 1680ms and 1700ms time intervals.

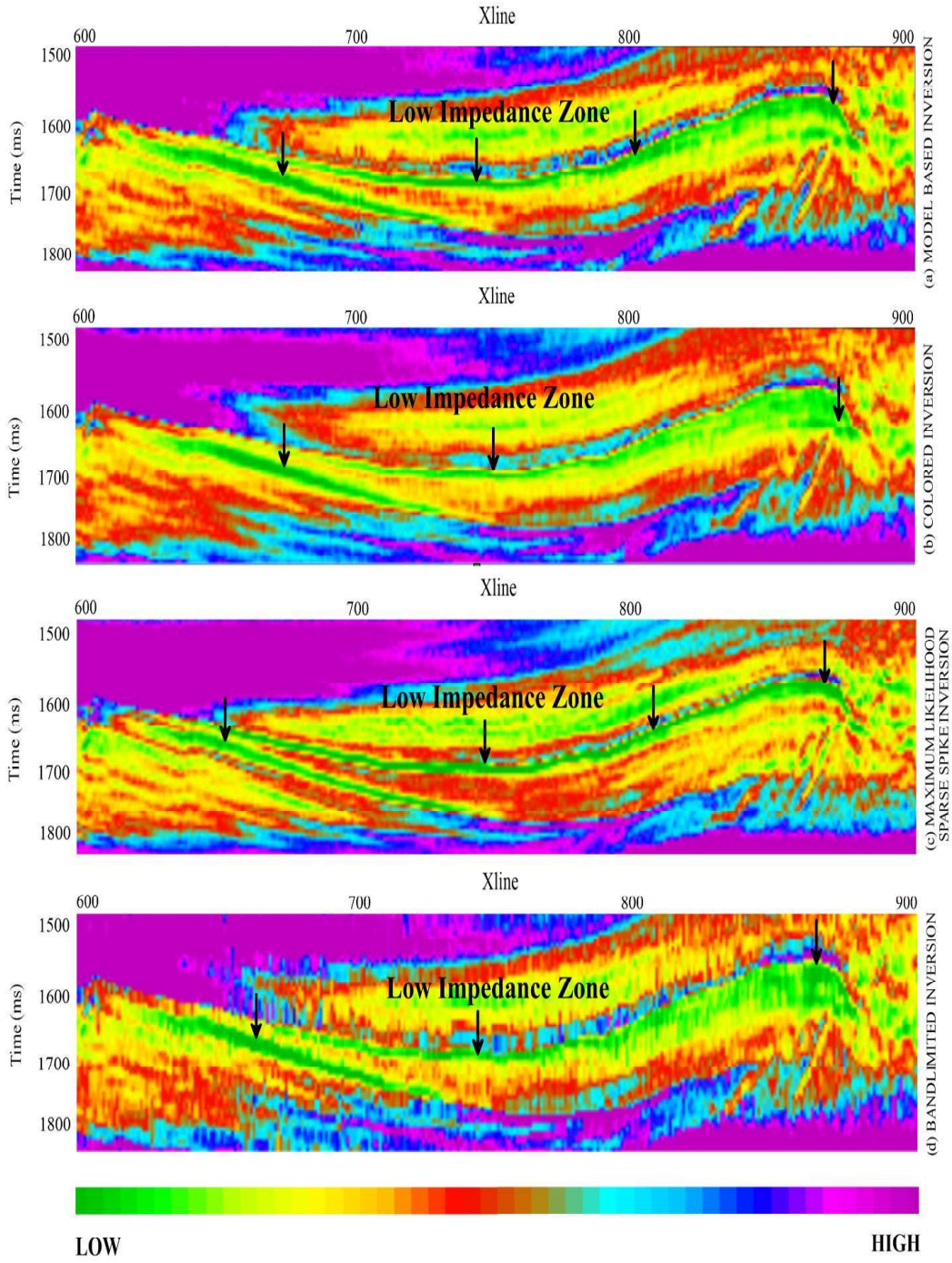

FIGURE 6.1: Estimated acoustic impedance using (a) model based inversion, (b) colored inversion, (c) maximum likelihood sparse spike inversion, and (d) bandlimited inversion method

Different techniques of spatial interpolation have been found to influence the variations

in the shapes of the time slices and the reservoir zone.
Given all these, MBI method has been intensively used to analyze and predict the geophysical parameters by different techniques.

6.2 Pre-stack inversion

6.2.1 Simultaneous inversion

The pre-stack seismic inversion has been done on Penobscot data, Canada, for determination of Z_P, Z_P, density (ρ), V_P, V_S and V_P/V_S ratio variations, by Simultaneous Inversion (SI) method. However, a comparison of the post- and pre-stack inverted results was not possible because SI has been performed on the pre-stack seismic data from the Penobscot whereas post-stack inversion is performed on the F3 block, the Netherlands.

A comparison between raw and conditioned pre-stack gather has been performed to show the effectiveness of conditioned gather. The differences between inverted raw and conditioned gather are illustrated in Figs. 6.2, 6.3, 6.4, 6.5, 6.6, and 6.7 for P-impedance, S-impedance, density, P-wave, S-wave and V_P/V_S ratio, respectively. The major changes in the Z_P, Z_P, density (ρ), V_P, V_S and V_P/V_S ratio between raw and conditioned gather is highlighted from green to yellow color in Figs. 6.2, 6.3, 6.4, 6.5, 6.6, and 6.7, respectively. The maximum changes in inverted values of Z_P, Z_P, density(ρ), V_P, V_S and V_P/V_S ratio and the corresponding time interval of these changes are clearly visible in Figs. 6.2-6.7, respectively. The changes are attributable to the presence of high amplitude seismic traces, which create significant differences in the gathers. For further understanding of data conditioning on geophysical parameters, horizon slice comparisons for raw and conditioned data at 2500ms can be scrutinized as revealed in Fig. 6.8.

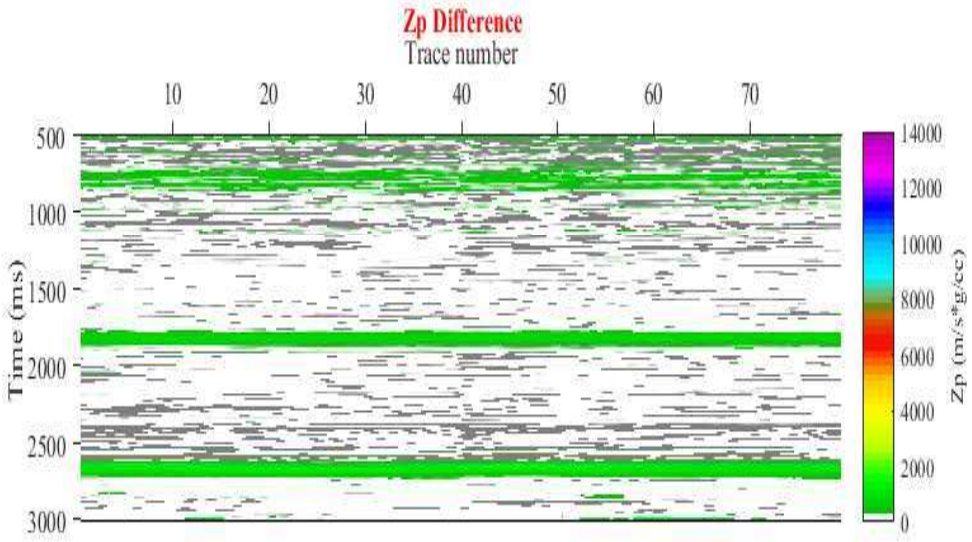

FIGURE 6.2: Difference between inverted P-impedance derived from conditioned and raw data

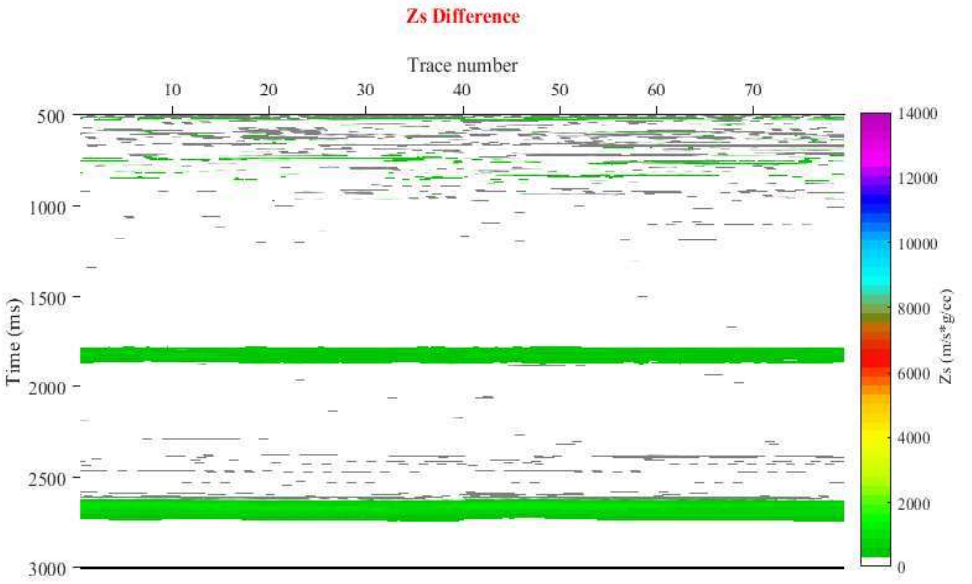

FIGURE 6.3: Difference between inverted S-impedance derived from conditioned and raw data

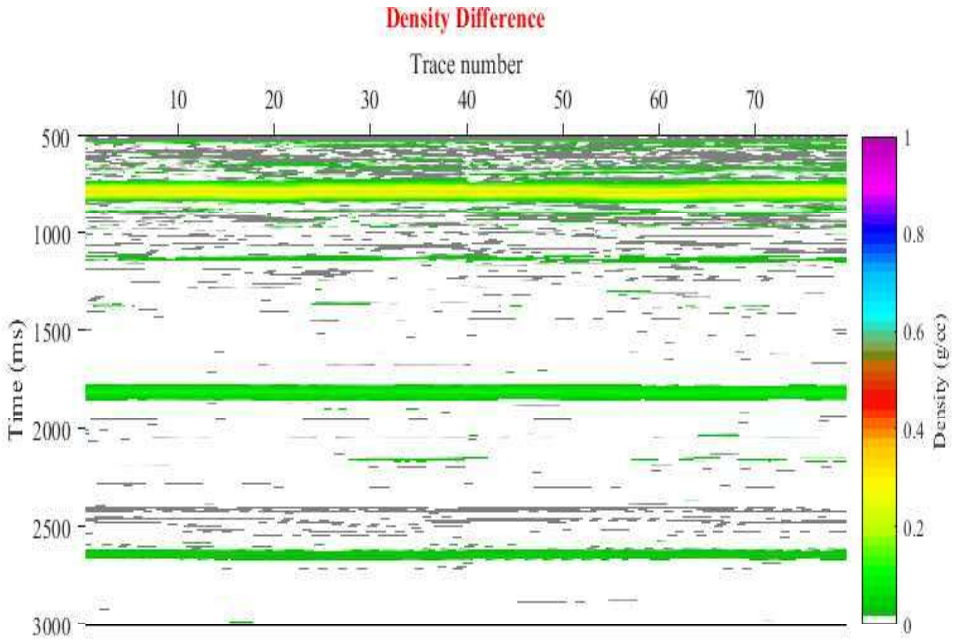

FIGURE 6.4: Difference between inverted density derived from conditioned and raw data

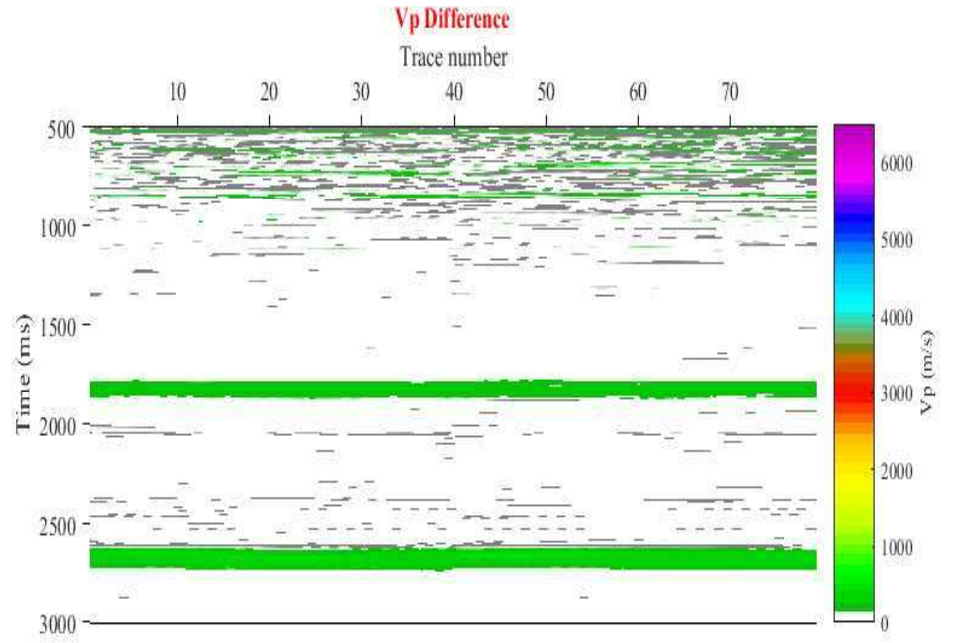

FIGURE 6.5: Difference between inverted P-wave velocity derived from conditioned and raw data

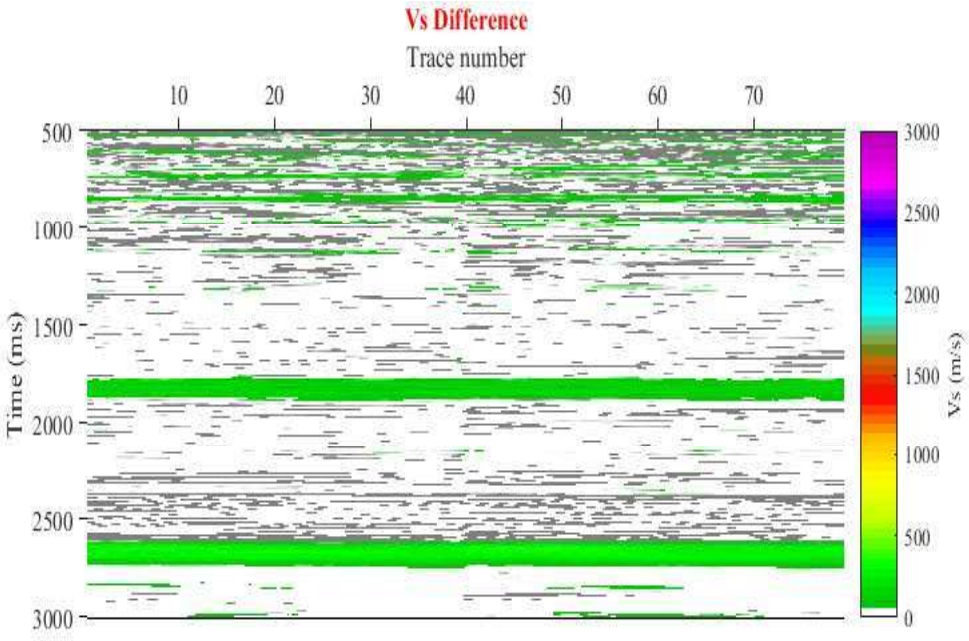

FIGURE 6.6: Difference between inverted S-wave velocity derived from conditioned and raw data

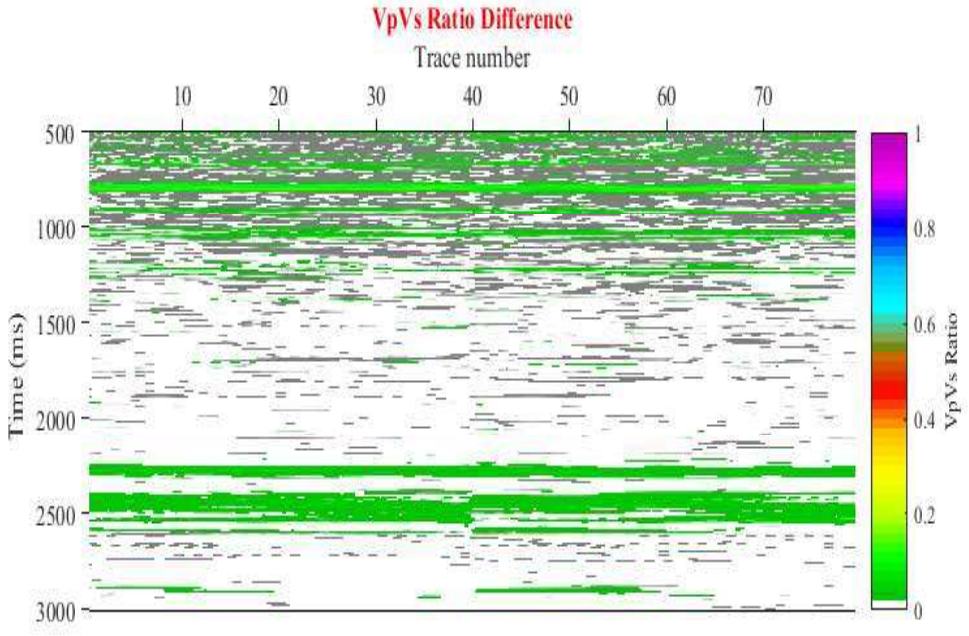

FIGURE 6.7: Difference between inverted V_P/V_S ratio derived from conditioned and raw data

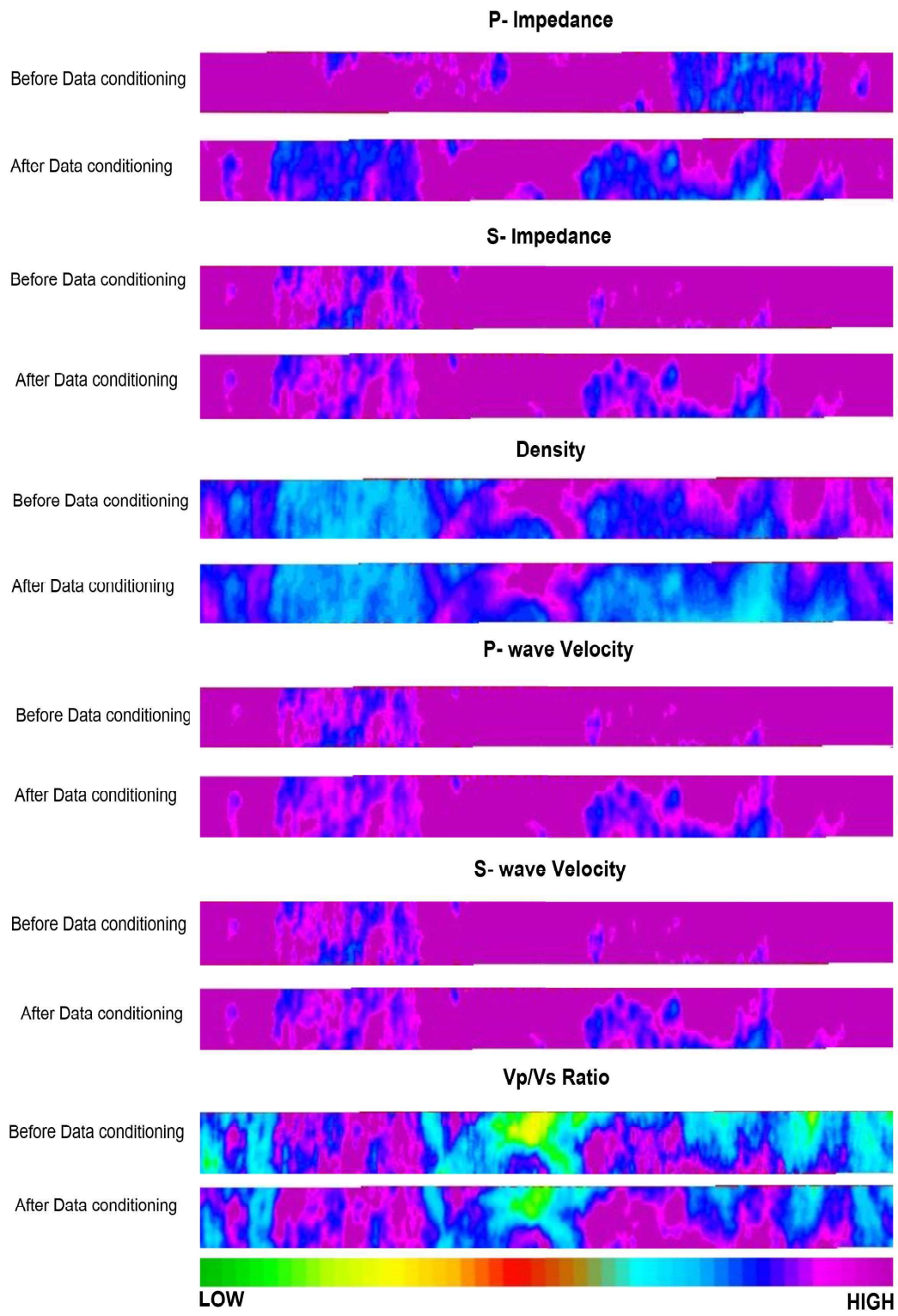

FIGURE 6.8: Data slice comparison between raw and conditioned data at 2500ms

SI reveals the non-existence of a significant reservoir in the Penobscot basin.

6.2.2 LMR transform

LMR transform derives lambda-rho and mu-rho by using inverted P-impedance and S-impedance, respectively. The differences between raw and conditioned gather for lambda- rho and mu-rho transform are illustrated in Figs. 6.9 and 6.10. The major lambda-rho differences between raw and conditioned gather at 700ms, 1800ms time intervals are observed in Fig. 6.9. The major mu-rho differences between raw and conditioned gather are shown in Fig. 6.10 at 1800ms and 2700ms time intervals.

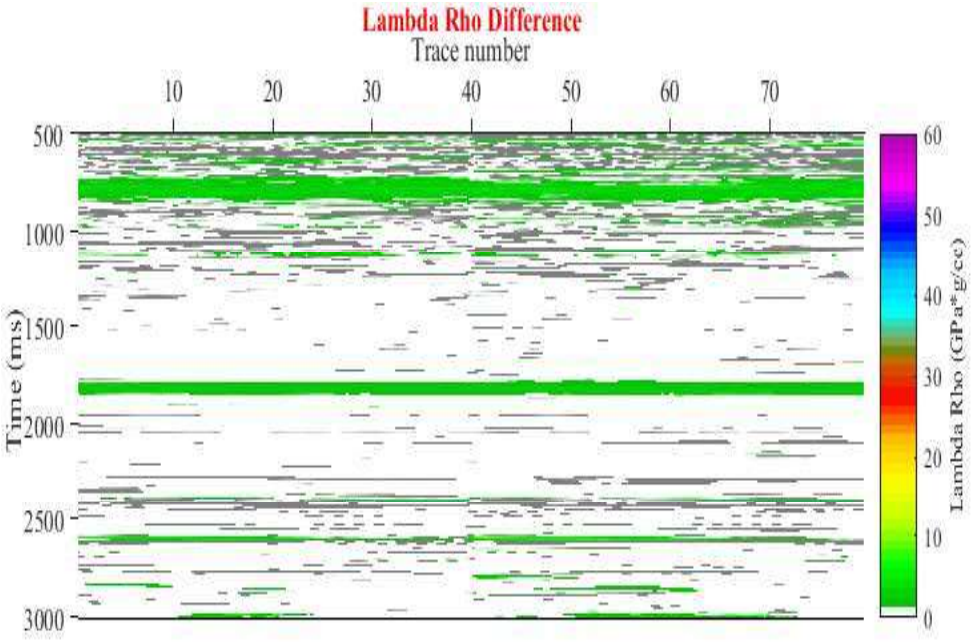

FIGURE 6.9: Difference between inverted lambda-rho derived from conditioned and raw data

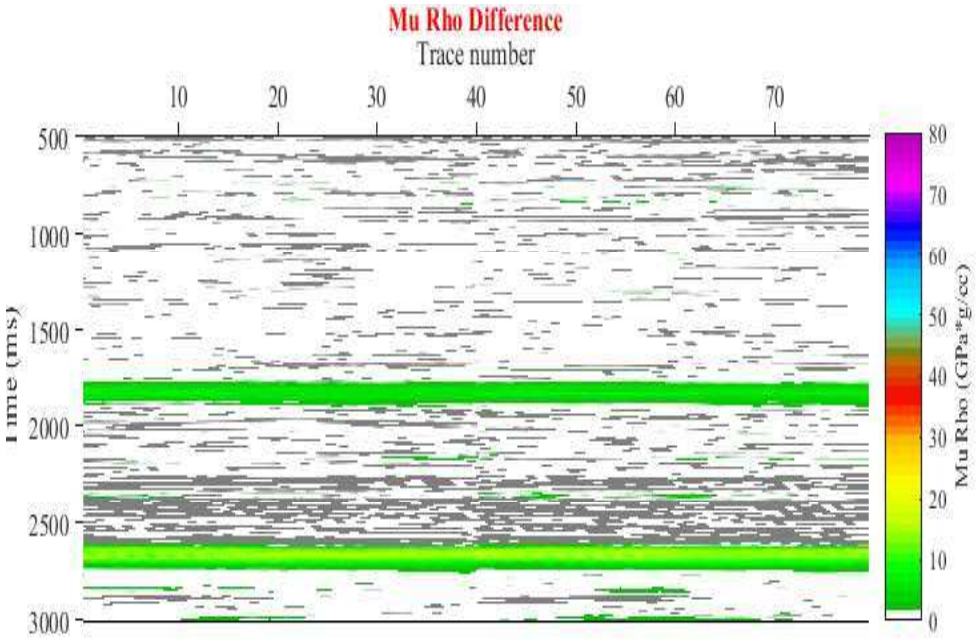

FIGURE 6.10: Difference between inverted mu-rho derived from conditioned and raw data

The crossplot generated from all these parameters (raw and conditioned gather) is given in Figs. 6.11. The cross plots among the inverted petrophysical parameters helped in establishing the relationship among them, which is very useful to estimate petrophysical parameters directly in this region. Both sections (raw and conditioned gather) show a slightly different relationship. However, average equations considering both the cases are given:

$$V_S = 0.8V_P - 850 \tag{6.1}$$

$$Z_S = 0.74Z_P - 15500 \tag{6.2}$$

$$Z_P = -8200\frac{V_P}{V_S} + 24000 \tag{6.3}$$

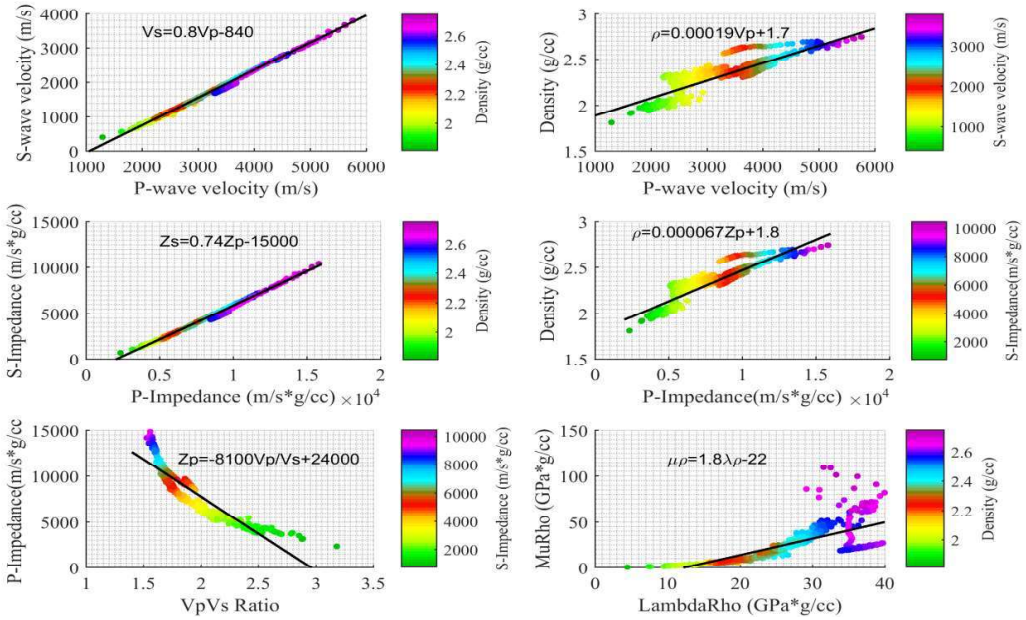

(A)

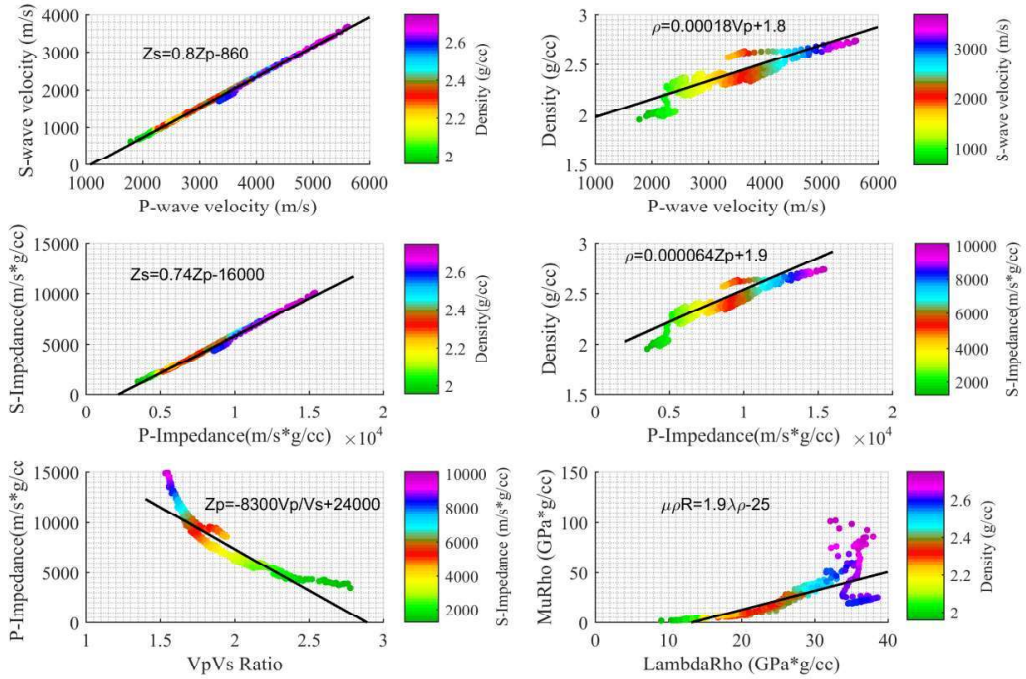

(B)

FIGURE 6.11: (a) Crossplots obtained from raw data and (b) Crossplots obtained from conditioned data

6.2.3 Elastic impedance inversion

The seismic reflection data from the Penobscot, Canada, was used for the investigation of elastic impedance in two phases. In the first phase, the investigation was conducted on synthetic data without noise and with incremental (10%, 20% and 30%) Gaussian noise. The study has revealed that the effectiveness of elastic impedance inversion (EI) drops by 3.5% with the addition of 30% noise in the data compared to data without noise. In the second phase, EI was applied on the original seismic data and its impact on near-angle stack gather as well as far-angle stack gather was computed. From the Figs. 5.54 and 5.55, it is observed that the correlation coefficients decreased and RMS error increased after adding 10%, 20% and 30% Gaussian noise. Therefore, it may be assumed as negligible. Fig. 5.56 reveals that the S/N ratio increases due to stacking which is usual, but it is also noteworthy that the resolution of far stack section increases much more as compared to the near stack gather. The comparison of EI derived results with the addition of Gaussian noise has been shown in Table 6.1.

TABLE 6.1: Comparison of EI derived results with the addition of Gaussian noise

Synthetic data	Correlation coefficient	Error
Zero noise level	0.998	0.019
10% noise level	0.992	0.092
20% noise level	0.982	0.190
30% noise level	0.963	0.265

After preparing the data, EI was again implemented into data in two phases. In the first phase, one composite trace close to well location was extracted from near as well as far angle stack gather and an inversion was performed on this trace to compare its results with well log data.

Fig. 5.57 depicts a comparison of inverted elastic impedance from the near stack as well as a far stack with well log impedance. From Fig. 5.57, it is observed that the inverted elastic impedance for the near stack as well as far stack is matching closely with well log elastic impedance. It is observed from Fig. 5.58 that for both cases (near

and far angle stack), the maximum number of scatter points lie close to the best fit line. This testifies the suitability of the algorithm for the given case.

In the second phase, the entire seismic section is inverted as represented by the cross-section in Fig. 5.61. The difference between near and far angle stack elastic impedance sections is discernible as highlighted by the arrow. The improved reflector resolution is higher in far stack elastic impedance section as compared to the near stack elastic impedance section. A crossplot of the near stack and far stack elastic impedance has been generated for entire datasets with inverted acoustic impedance as a color bar (Fig. 5.62). There is an absence of cluster points, which shows a different variation of near and far stack elastic impedance. Therefore, it may be inferred that the region does not contain any considerable gas formation.

6.3 Geostatistical techniques

Single attribute analysis, multi attribute analysis, probabilistic neural network (PNN) and multilayer feed forward network (MLFN) have been effectively used to estimate log properties using seismic attributes. The predicted porosity, density, P-wave and gamma ray logs yielded a good correlation of 0.95. 0.94, 0.93 and 0.79, respectively, for application of multi-attribute regression with MBI as an external attribute. Therefore, MBI derived impedance is used as an external attribute for geostatistical techniques to predict petrophysical parameters.

The predicted porosity, density, P-wave and gamma ray logs showed a high correlation of 0.97. 0.96, 0.95 and 0.82, respectively with PNN as a prediction tool and MBI as external attributes and it is 0.96, 095, 0.94 and 0.80 with MLFN as a prediction tool and MBI as an external attribute.

PNN and MLFN generated predicted volumes are illustrated in Figs. 6.12 and 6.13, respectively. The anomalous zones are highlighted by an ellipse in Figs. 6.12 and 6.13. The predicted volumes from PNN algorithm gave a slightly better resolution than MLFN predicted volumes. The crossplots using PNN with MBI as an external attribute are represented in Figs. 6.14 (c-d). These cross plots have clearly indicated

the anomalous zone. Fig. 6.14e reveals the anomalous area in the seismic section. The predicted sections show very high-resolution subsurface information as compared to the input seismic data. The predicted curves have been compared with the original curves, which exhibit a good match with good correlation. This geostatistical predicted section is more informative as compared to the seismic data because of two reasons; firstly, the section is providing layer property whereas the seismic data provides interface properties and secondly, it interpolates the well log property into the seismic sections to provide detailed information. An anomalous zone is found near the 1700ms time interval.

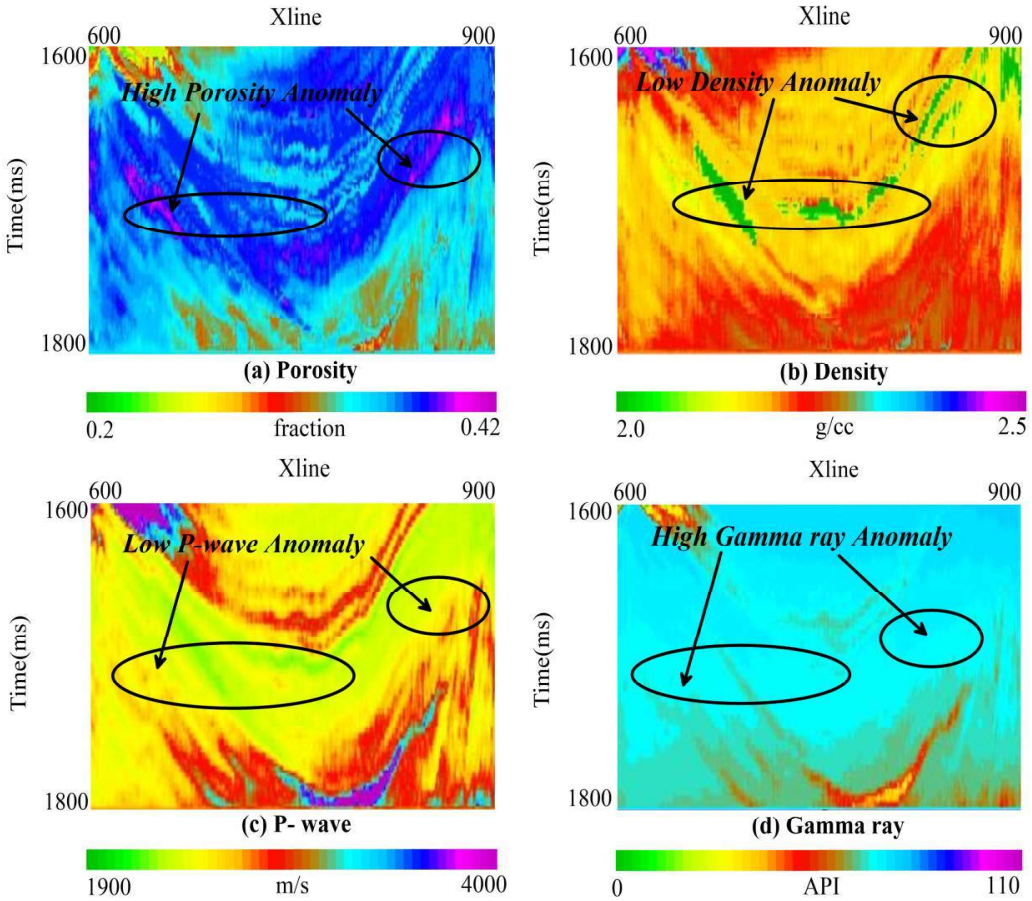

FIGURE 6.12: Predicted volumes using PNN for (a) porosity, (b) density, (c) P-wave and (d) gamma ray (Inline 244)

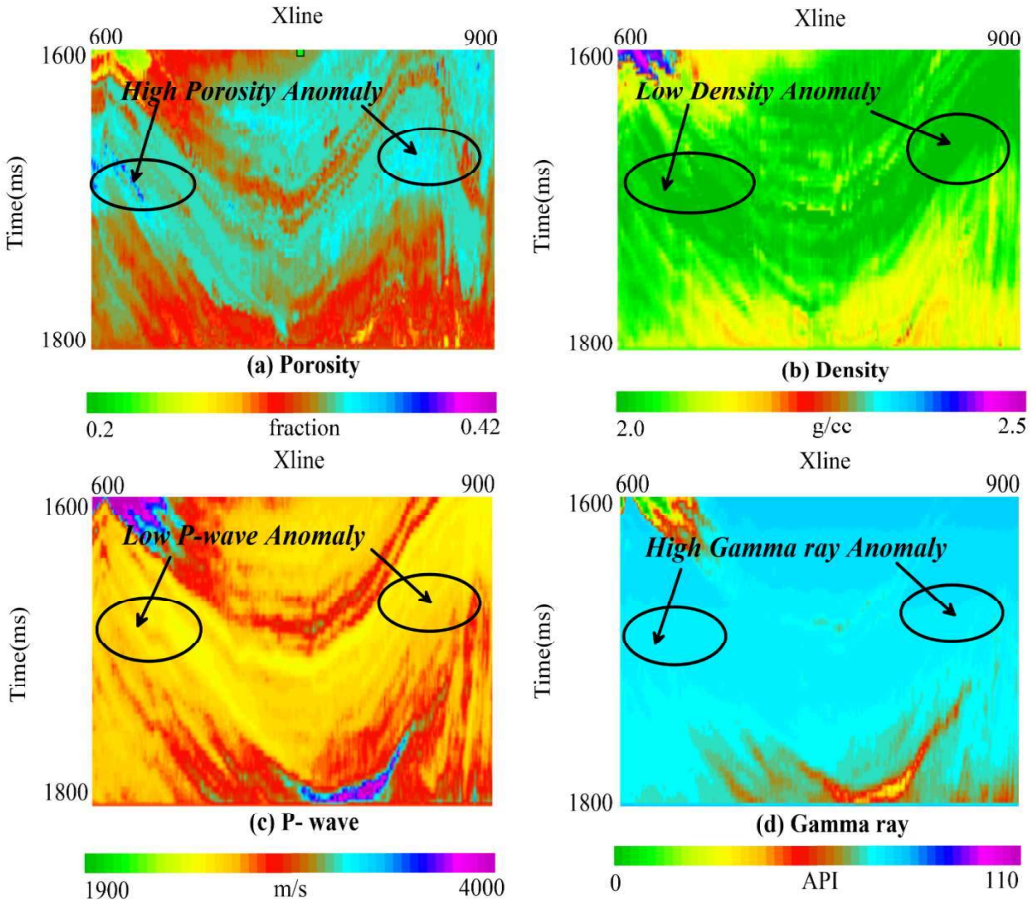

FIGURE 6.13: Predicted volumes using MLFN for (a) porosity, (b) density, (c) P-wave and (d) gamma ray (Inline 244)

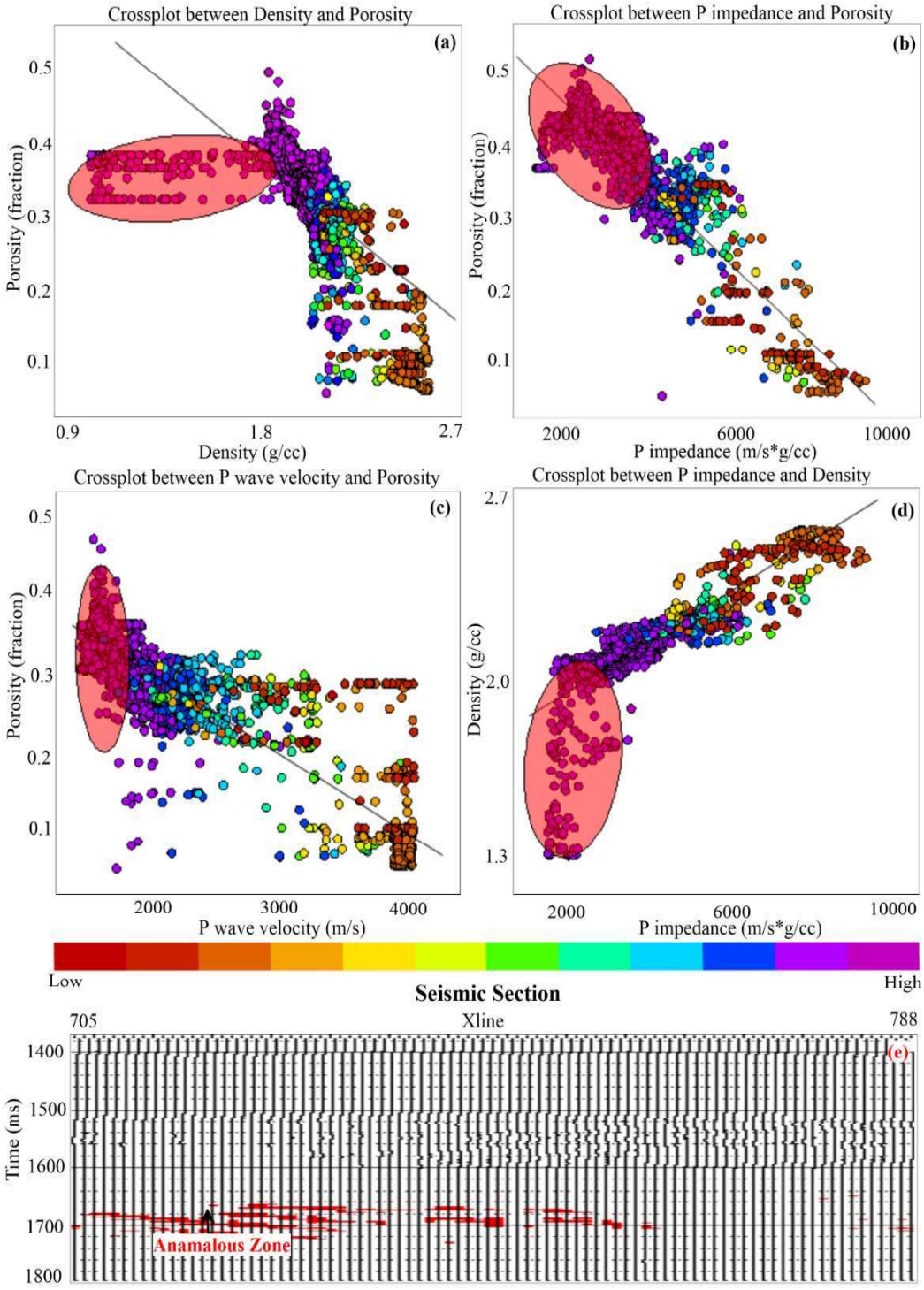

FIGURE 6.14: Crossplot between (a) density and porosity, (b) P- impedance and porosity, (c) P- wave velocity and porosity, (d) P-impedance and density and (e) Cross-section of seismic data highlights anomalous zone

TABLE 6.2: Holistic comparison of the results from post-stack inversion methods

Properties	**MBI**	**CI**	**MLSSI**	**BLI**
Inpedance(m/s*g/cc)	**2500-6200**	2600-6350	2550-6400	2700-6500
Average Correlation	**0.99**	0.81	0.88	0.87
Residual Error(g/cc*m/s)	**359.55**	513.68	361.39	444.65
Synthetir Relative Error	**0.153**	-	0.430	-
Amplitude spectra correlation	**0.97**	0.92	0.96	0.95

PNN and MLFN provide better prediction results than single and multi-attribute analysis because PNN and MLFN use non-linear relationship attributes while single and multi attribute analysis uses the linear relationship between the target log and the attributes.

PNN, in conjunction with MBI impedance as an external attribute, has displayed better performance of the algorithm as compared to the MLFN derived impedance algorithm using MBI as an external attribute (Fig. 6.12 and 6.13). Therefore, it may be understood that PNN technique is the best method to predict the petrophysical parameters for the given 3D post-stack seismic data.

Tables 6.2 and 6.3 represent holistic comparison of results obtained from all inversion methods and geostatistical techniques, respectively. Column 1 (Table 6.2) reveals the estimated properties for reservoir zone; column 2 to 5 represents the inversion methods used in the present study. Colomn 1 (Table 6.3) reveals predicted properties using geostatistical techniques; column 2 represents techniques used in the present study.

The above table reveals that the impedance (2500-6200m/s*g/cc) in the reservoir zone is the smallest for MBI. The correlation coefficient (0.99) is the highest and residual error (449.79) is the least for model-based inversion. This indicates the most accurate inverted results. Indeed, in the model-based inversion case, the amplitudes in inverted impedance and seismic data suggest that the amplitudes and frequencies are preserved. The cross-correlations (0.97, 0.96, 0.95 and 0.82) between original and predicted petrophysical parameters (porosity, density, P-wave and gamma ray, respectively) are highest for the probabilistic neural network when impedance derived from

TABLE 6.3: Holistic comparison of the results obtained from geostatistical techniques

Properties	**Multi attribute analysis**	
	Correlation	Error
Porosity	0.95	0.015
Density	0.94	0.048
P-wave	0.93	78.44
Gamma ray	0.79	13.18
Properties	**PNN**	
	Correlation	Error
Porosity	**0.97**	**0.014**
Density	**0.96**	**0.046**
P-wave	**0.95**	**70.88**
Gamma ray	**0.82**	**13.05**
Properties	**MLFN**	
	Correlation	Error
Porosity	0.96	0.020
Density	0.95	0.051
P-wave	0.94	73.00
Gamma ray	0.80	13.13

MBI is utilized as an external attribute. This indicates that PNN algorithm, in conjunction with MBI method, is the most accurate in the prediction of petrophysical parameters volumes (porosity, density, P-wave and gamma ray) for post-stack seismic data.

The results obtained from post-stack inversion methods and geostatistical techniques for post-stack data have clearly revealed appropriate findings for the existence of reservoirs between 1680ms to 1700ms time intervals. This time interval zone is equivalent to 1680m of the depth of occurrence of the reservoir, from the ground surface. The horizontal and vertical extents of the reservoir have been determined from the inline and crossline. The reservoir exists from inlines 200-300 and from crosslines 630-880. Therefore, the horizontal extent of the reservoir in inline and crossline directions may be estimated as 3687m and 4445m, respectively.

For the pre-stack data, various seismic inversion methods used in the estimation of petrophysical properties of this field have been unable to detect any reservoir present in the study area.